Light Metals 2015
Edited by: Margaret Hyland
TMS (The Minerals, Metals & Materials Society), 2015

Light Metals 2015

ALUMINUM ALLOYS: DEVELOPMENT, CHARACTERIZATION AND APPLICATIONS

Simulation and Modeling

SESSION CHAIR
Grant Chen
Université du Québec à Chicoutimi
Chicoutimi, Quebec, Canada

Light Metals 2015
Edited by: Margaret Hyland
TMS (The Minerals, Metals & Materials Society), 2015

DEFORMATION AND FAILURE OF AN Al-Mg ALLOY INVESTIGATED THROUGH MULTISCALE MICROSTRUCTURAL MODELS

Andrew C. Magee[1] and Leila Ladani[1]
[1]Department of Mechanical Engineering, University of Connecticut, Storrs, USA

Keywords: crystal plasticity, cohesive interface, bimodal alloys, Al-Mg

Abstract

The microscale deformation of an Al-Mg alloy with a bimodal grain size distribution, consisting of coarse grains (CGs) and ultrafine grains (UFGs) is studied through finite element methods. Procedurally generated models are created to characterize the behavior of this microstructure at different scales. The mechanical response of individual grains is represented through crystal plasticity laws, which include accommodations for solute and grain size strengthening effects. These effects are quantified through multiscale models allowing for experimental calibration. Additionally, the behavior of grain boundaries is included through cohesive interface models. Using these techniques, grain scale deformation is characterized, load distribution between the two phases is examined, and the roles of crystal anisotropy and interface accommodation are considered.

Introduction

Bimodal grain size alloys were introduced to overcome the issues associated with ultrafine grain and nanostructured material such as low ductility. Addition of course grains to the ultrafine grain and nanostructures is expected to enhance the ductility[1–6]. As expected at the grain level, the properties of the two regions with different grain sizes are dramatically different. This leads to complex stress and strain contours in the microstructure, complicating the deformation and failure behavior of the material. Bimodal microstructures have been utilized for many material systems, but Al-Mg is a commonly studied one. This work is based on experimental data collected in uniaxial tensile tests of ultrafine grain Al 5083 with 10% CG (by volume). Material examined in this study consists of equiaxed UFGs approximately 100 nm in diameter and discrete CG regions elongated in the extrusion direction with a grain size of about 1 μm [7].

To study the behavior of this material, and to understand the emergent behavior attributable to the two different phases, finite element methods are commonly employed. Previously, these models have been idealized representations of the microstructure, to provide high level information on the material's behavior. Models depicting a bimodal "unit cell," a quarter-symmetric circular CG embedded in a homogeneous UFG region, have predicted crack initiation at CG/UFG interfaces, due to the large differences in the phases' properties, followed by propagation normal to the loading direction [8]. Other models have captured the overall extruded structure of the material, showing failure initiation at an interface followed by propagation through UFG and CG regions [9]. These models have captured large scale mechanisms active in the material, and although they differentiate between the CG and UFG phases, inside of these regions they are treated as isotropic and homogeneous. At the grain scale, these assumptions may no longer be appropriate due to the anisotropy attributable to the crystalline structure of the individual grains as well as the increased influence of grain boundaries at smaller scales. In the literature, constitutive equations have been developed to address these features and are implemented in this study. Crystal plasticity methods are used to capture the orientation dependent elastic and plastic response of grains modeled as single crystals separated by grain boundaries represented as cohesive interfaces.

Most crystal plasticity models used for microstructural analyses couple crystal plasticity with grain boundary models [10–12]. There are several approaches to the treatment of grain boundaries. Depending on the scale of the model, grain boundaries can be treated as discrete regions of the model or as interfaces between grain structures. When modeled as regions, several approaches have been taken, from defining the grain boundary regions through more traditional plasticity methods such as Voce hardening, to applying crystal plasticity to these areas as well with a different set of material constants to reflect the properties of the boundary [13–15]. Alternatively, grain boundary elasticity, plasticity, and failure can be represented through traction-displacement relationships applied to cohesive interfaces between grains [10,16,17].

In this work, a crystal plasticity model is adapted for use with UFG Al 5083 by adjusting the material constants of the model to account for solute and grain size strengthening effects. A grain boundary model previously used in [18] is applied to the cohesive interfaces between grains. Procedurally generated large scale and grain scale finite element models of the bimodal structure are used to study the loading and intergranular failure behavior of this material.

Plasticity Models

Crystal plasticity is applied inside of the grains using the general concepts of crystal plasticity finite element methods. The individual grains of the polycrystal model are represented as single crystals through crystal plasticity methods. In this work, crystal plasticity methods are used to evaluate the non-isotropic mechanical response of the grains at the microstructural level due to their crystalline nature. The general equation given by Marin in [19] is used to obtain the slip rate:

$$\dot{\gamma}^{\alpha} = \dot{\gamma}_0 \exp\left\{\frac{-\Delta F}{k\theta}\left[1-\left(\left|\frac{\tau^{\alpha}}{g_c^{\alpha}}\right|\right)^{p}\right]^{q}\right\}\mathrm{sgn}(\tau^{\alpha}) \quad (1)$$

where $\dot{\gamma}_0$ is a reference strain rate, ΔF is the activation free energy required to overcome slip obstacles without applied stresses, k is the Boltzmann constant, θ is temperature, τ^{α} is the resolved shear stress on slip system α, g_c^{α} is the total resistance to slip, and p and q are constants describing the shape of the glide resistance profile.

To describe the strain hardening of the crystal, the slip resistances must also be updated for each iteration. This is done,

again following Marin's approach. The material constants necessary for his model are readily available for pure aluminum [19,20]. To extend this model to alloys, and further to UFGs, the approach used by Pouiller et al. is employed and extended. Here, it is assumed that the slip system strength is the additive combination of the pure crystal's behavior and solute strengthening effects [20]. This method handles the grain size effects in a much simpler fashion, at the cost of generality and the requirement of the determination of suitable factors. A method for extracting these factors from experimental data is described in the next section.

For the grain boundaries, a cohesive interface model based on the one presented by Wei and Anand in [10] is used. Grain boundaries are modeled through an elastic-plastic traction-displacement relationship with power law hardening. As shown in Figure 1, the elastic region is defined by the constants K, the interfacial elastic stiffness, and s_0, the critical strength. The model differentiates between grain boundary deformation normal and tangential to the interface, so these parameters can vary between the two modes. In the elastic region, K_N corresponds to the normal direction and is calculated from the elastic modulus, and K_T is the value in the tangential direction and is calculated from the shear modulus [10,18]. The plastic region is described by the hardening law

$$t = a\bar{\delta}^n \tag{2}$$

where t is the traction, $\bar{\delta}$ is the total plastic displacement, and a and n are material constants which are taken to be the same in both deformation modes. The total plastic displacement is a combination of displacement in the normal and tangential directions according to

$$\bar{\delta} = \sqrt{\delta_N^2 + \alpha\delta_T^2}\ . \tag{3}$$

with coupling parameter $\alpha = 0.25$. Finally, a plastic displacement-based failure criterion γ_{fail} can be enforced. At the initiation of failure, the interfacial stress degrades according to the constant C_{fail}. The grain boundary model used in this study is examined in more detail in [18].

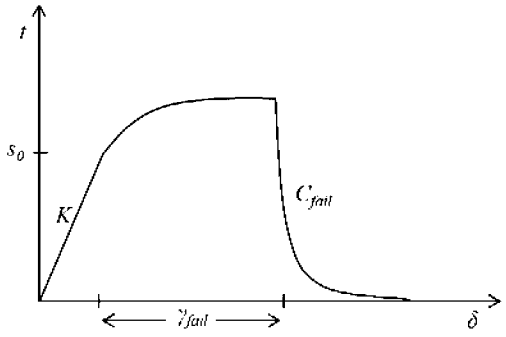

Figure 1. Grain boundary traction-displacement relationship.

Implementation of the Model

To use these descriptions of grain boundaries and interiors in the study of the grain level loading and deformation effects in this material, a small scale model incorporating the interactions of both CG and UFG phases is required. Representing the differences in the two regions through different sets of material constants is a straightforward idea, but is limited by the availability of such data. While a wealth of data is available for pure metals and common alloys, from which the necessary constants from the previous section can be extracted, it is more difficult to find representations for the effects of decreased grain size present in the UFG phase. Therefore, a multiscale modeling technique utilizing data available in the literature and experimentally obtained results was developed. First, a large scale model depicting a representative area of the entire bimodal material is created and matched to experimental data for a corresponding CG ratio by changing the properties of the UFG region (since the properties of the CG region are known from handbook Al 5083 data). Next, a small scale polycrystal model is generated. This model is used to match the conventional Al 5083 curve from literature. Starting from published values for pure Al, constants are added to the crystal plasticity parameters to represent the contribution of solute strengthening. Next, the polycrystal model is used in the same manner to match the curve for the UFG region from the large scale model, giving the effect of grain size. Finally, these two materials are combined into a polycrystalline model containing both CGs and UFGs.

A large scale model is necessary in this case because a model large enough to depict a representative area would have a prohibitively large number of individual UFGs. Conversely, a model that can represent individual grains and the interaction of the two phases is not representative of the macroscopic mechanical behavior depicted in a tensile test. In the large scale model shown in Figure 2, and all other finite element models in this work, the left edge is fixed and a tensile displacement condition is applied to the right edge. Additionally, all nodes are fixed in the out of plane direction.

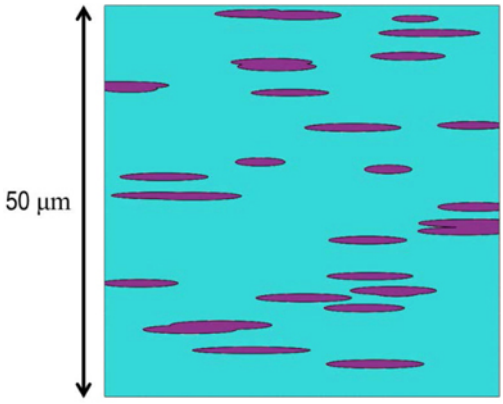

Figure 2. Large scale model (9% CG by area). CGs are randomly generated in random locations with a random size

With the elastic-plastic properties of the CG phase readily available in literature [21,22], it thus remains to vary the UFG region to match the experimental results for the bimodal material. For both CG and UFG phases an isotropic elastic modulus E of 70 GPa was used [22]. The experimental results, shown in Figure 3, are the average of three uniaxial tensile tests performed at a strain rate of 10^{-4} s^{-1}. The values of the constants extracted from the model fitting are given in Table 1. In all such model fitting work, the question of uniqueness invariably arises. To address this, initial guesses for these parameters were obtained through extrapolation from the experimentally measured values for 10-30% CG ratio to a 0% CG material. Since the values obtained in this manner are physically plausible, it is expected to put the problem in the correct "basin of attraction." Furthermore, the

constants varied in this study have distinct effects on the resultant stress-strain curve, which can be adjusted to match the different features of the experimental data. Therefore it is expected that the values for constants obtained through model fitting are suitable in the conditions modeled. In this manner, the large scale properties of the UFG region are determined and can now be used to obtain the parameters for the crystal plasticity model.

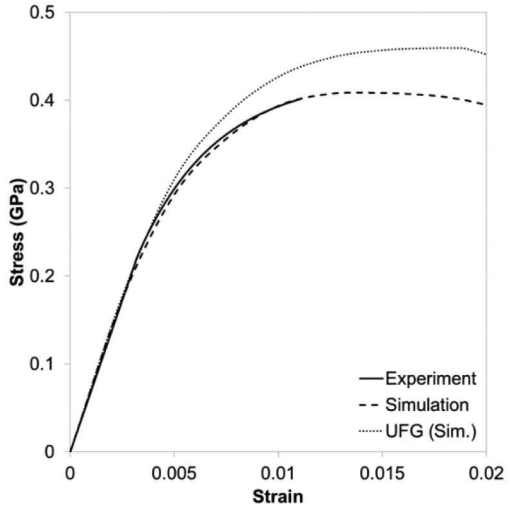

Figure 3. Stress-strain curves of the large scale CG/UFG model fit to 10% CG experimental data and the resultant curve for the UFG region.

Table 1. Material properties for UFG Al 5083 in large scale model.

Property	Value
E [GPa]	70
σ_y [MPa]	275
σ_s [MPa]	470
ε_c	0.0025

Next, to determine the values for the crystal plasticity model for both the UFG and CG regions, a small scale model was developed. Crystallographic orientations are uniformly randomly assigned to each grain, in accordance with experimental observations of randomly oriented grains [7].

The crystal plasticity and grain boundary models described in Section 2 were used in this model. To extract the material properties for the crystal plasticity description, the stress-strain results from this model were fit to experimental data in the case of the CGs or to the output of the large scale model for the UFGs. Other properties of the crystal and interface models were the same between the two phases, with the values shown in Table 2.

Table 2. Material properties for both CG and UFG phases.

Elasticity (GPa) [23]		**Crystal Plasticity**		**Interface**	
C_{11}	106.49	$\dot{\gamma}_o$	1×10^{-3} s^{-1}	K_N	70 GPa
C_{12}	60.39	$\dot{\gamma}_{so}$	5×10^{10} s^{-1}	K_T	26 GPa
C_{14}	28.28	ΔF	3×10^{-19} J	s_0	509 MPa
		p	0.141	a	181 MPa
		q	1.1	n	0.4

To investigate the grain level interaction of the CG and UFG regions, two coarse grains were added to the model shown in Figure 4. The two phases were described by the crystal plasticity model with the appropriate constants as determined above. This bimodal model, shown in Figure 4, can now be used to examine the local interaction behavior between the CG and UFG phases.

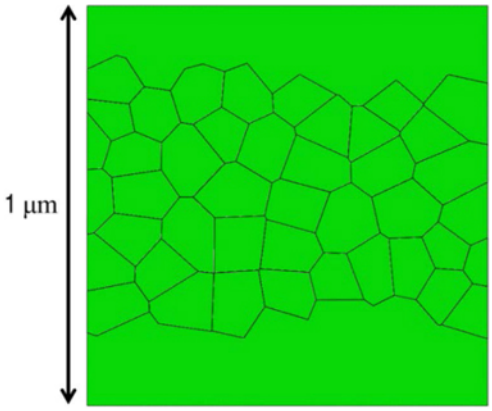

Figure 4. Grain level model with two CGs separated by a UFG region.

Results

The stress and strain contours in the large scale bimodal model are shown in Figure 5. It can be seen that stresses are concentrated in the UFG region, with relaxation regions occurring at the tips of the CGs. Strain is mostly concentrated in bands between CG regions, with the highest values occurring in the UFG matrix between closely spaced CGs. For a strain-limited failure, as is expected for this material, this would indicate damage initiation at these sites. Therefore, the small scale model in Figure 4 with its closely spaced CG regions is a good tool for the study of damage initiation effects, even if it is not representative of the entire microstructure.

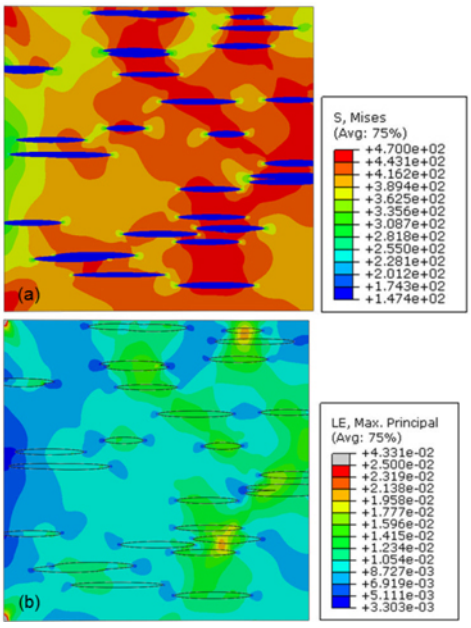

Figure 5. Stress, in MPa, (a) and strain (b) distributions in the large scale bimodal model.

The features of the simulation are consistent with experimental observations of the fracture surface in tension, which showed a ductile type failure texture and load segregation between the two phases [7,24]. Micrographs also showed failure occurring through CG regions, as opposed to interfacial delamination with the UFG matrix [7]. This is consistent with the model results, with failure originating in the high strain sites and transferring load to the CGs and the UFG matrix loses its load bearing capacity and the crack begins to propagate.

The small scale bimodal model was run using the crystal plasticity and isotropic (with material properties from the large scale model) descriptions of the phases, with and without the grain boundary model. The stress-strain curves from these trials, generated from the reaction forces and displacement of the edge with the displacement boundary condition, are shown in Figure 6. It can be seen that inclusion of the grain boundary model resulted in reduced stresses, owing to the added compliance of the grain boundary region when compared to rigidly attached grains. It is also apparent that the isotropic model consistently predicts a higher stress-strain response than the crystal plasticity description, probably due to the low strength exhibited by some crystallographic orientations that the isotropic model does not account for.

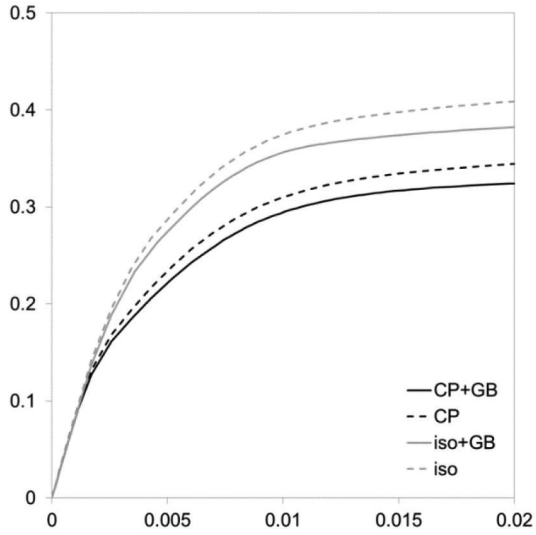

Figure 6. Stress-strain curves for crystal plasticity (CP) and isotropic (iso) models, with and without grain boundaries (GB).

The plots of grain boundary displacement in Figure 7 show that the sites of high interfacial displacements were generally the same in both the crystal plasticity and isotropic models. These sites lay on the CG/UFG interface, with their maxima on the interface and decreasing with distance into the UFG matrix. The two models did not show the same magnitude of displacements, however. That is, while boundary motion tended to be concentrated in the same areas in both models, the actual amount of deformation in these areas was not the same. The crystal plasticity model tended to distribute lower amounts of deformation across more sites, while the isotropic one produced more concentrated distributions. By comparing the total deformation in the boundaries to the applied displacement on the model, it is estimated that the interfaces account for as much as 40% of the total deformation.

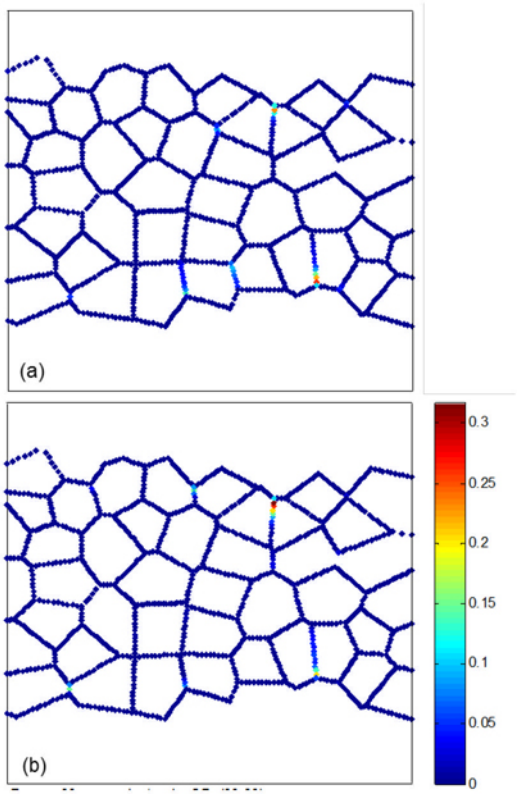

Figure 7. Total plastic displacement at grain boundaries (nm) in (a) crystal plasticity model and (b) isotropic model.

Comparison of the two plots in Figure 7 shows that the initiation of grain boundary failure is not dependent on the crystal orientation, since the sites of high deformation are similar in both plots. This suggests that grain boundary failure mechanisms may not be a direct result of grain deformation, but rather an independent event that is influenced by the configuration of the microstructure at the grain level.

This model highlights the role that the grain interfaces play in the material's deformation. Their inclusion serves to distribute strain more evenly across the microstructure, reducing concentrations and delaying the onset of failure, in addition to serving as failure initiation sites under some possible crack propagation cases. This suggests that engineering efforts directed at the properties of the grain boundaries could be utilized to improve the mechanical response of this and similar systems. Finally, it emphasizes the interactions between the grain interiors and boundaries over the course of loading and shows that both effects must be considered for an accurate microstructural representation.

Conclusion

The grain level microstructural deformation of a bimodal aluminum alloy was simulated through crystal plasticity finite element modeling with grain boundaries represented through cohesive interface models. The material properties for the UFG phases in these models were extracted from experimental data using known values for the CGs and a multiscale modeling approach. These models were procedurally generated to depict the relevant features of the microstructure at the scale of individual

grains as well as at a larger, statistically representative scale. It was found that the crystal plasticity model, considering the orientations of individual grains, predicted a weaker stress-strain response than an identical model whose grains behaved isotropically. Additionally, the inclusion of the grain boundary model served to further weaken the model due to the added compliance of these regions. The large and grain scale models showed high strain regions between closely spaced CG bands in the microstructure where cracks are likely to initiate at the CG/UFG interface and propagate into the UFG matrix perpendicular to the loading direction.

Acknowledgement

This work was supported by funding from CMMI-1416682 and CMMI-1053434.

References

1. Lee, Z., Witkin, D. B., Radmilovic, V., Lavernia, E. J., and Nutt, S. R. Bimodal microstructure and deformation of cryomilled bulk nanocrystalline Al–7.5Mg alloy. *Mater. Sci. Eng. A* 410-411, 462–467 (2005).
2. Witkin, D., Lee, Z., Rodriguez, R., Nutt, S., and Lavernia, E. Al–Mg alloy engineered with bimodal grain size for high strength and increased ductility. *Scr. Mater.* 49, 297–302 (2003).
3. Han, B. Q., Ye, J., Tang, F., Schoenung, J., and Lavernia, E. J. Processing and behavior of nanostructured metallic alloys and composites by cryomilling. *J. Mater. Sci.* 42, 1660–1672 (2007).
4. Topping, T. D., Ahn, B., Li, Y., Nutt, S. R., and Lavernia, E. J. Influence of Process Parameters on the Mechanical Behavior of an Ultrafine-Grained Al Alloy. *Metall. Mater. Trans. A* 43, 505–519 (2011).
5. Witkin, D. B., and Lavernia, E. J. Synthesis and mechanical behavior of nanostructured materials via cryomilling. *Prog. Mater. Sci.* 51, 1–60 (2006).
6. Youssef, K. M., Scattergood, R. O., Murty, K. L., and Koch, C. C. Nanocrystalline Al–Mg alloy with ultrahigh strength and good ductility. *Scr. Mater.* 54, 251–256 (2006).
7. Magee, A., Ladani, L., Topping, T. D., and Lavernia, E. J. Effects of tensile test parameters on the mechanical properties of a bimodal Al–Mg alloy. *Acta Mater.* 60, 5838–5849 (2012).
8. Ye, R. Q., Han, B. Q., and Lavernia, E. J. Simulation of Deformation and Failure Process in Bimodal Al Alloys. *Metall. Mater. Trans. A* 36, 1833–1840 (2005).
9. Nelson, S., Ladani, L., Topping, T., and Lavernia, E. Fatigue and monotonic loading crack nucleation and propagation in bimodal grain size aluminum alloy. *Acta Mater.* 59, 3550–3570 (2011).
10. Wei, Y., and Anand, L. Grain-boundary sliding and separation in polycrystalline metals: application to nanocrystalline fcc metals. *J. Mech. Phys. Solids* 52, 2587–2616 (2004).
11. Shaban, A., Ma, A., and Hartmaier, A. Polycrystalline material deformation modeling with grain boundary sliding and damage accumulation. *ECF18, Dresden 2010* 1–8 (2013).
12. Bower, A. F., and Wininger, E. A two-dimensional finite element method for simulating the constitutive response and microstructure of polycrystals during high temperature plastic deformation. *J. Mech. Phys. Solids* 52, 1289–1317 (2004).
13. Fu, H.-H., Benson, D. J., and André Meyers, M. Computational description of nanocrystalline deformation based on crystal plasticity. *Acta Mater.* 52, 4413–4425 (2004).
14. Schwaiger, R., Moser, B., Dao, M., Chollacoop, N., and Suresh, S. Some critical experiments on the strain-rate sensitivity of nanocrystalline nickel. *Acta Mater.* 51, 5159–5172 (2003).
15. Liu, Y., Zhou, J., and Hui, D. A strain-gradient plasticity theory of bimodal nanocrystalline materials with composite structure. *Compos. Part B Eng.* 43, 249–254 (2012).
16. Warner, D. H., Sansoz, F., and Molinari, J. F. Atomistic based continuum investigation of plastic deformation in nanocrystalline copper. *Int. J. Plast.* 22, 754–774 (2006).
17. Wu, B., Liang, L., Ma, H., and Wei, Y. A trans-scale model for size effects and intergranular fracture in nanocrystalline and ultra-fine polycrystalline metals. *Comput. Mater. Sci.* 57, 2–7 (2012).
18. Magee, A. C., and Ladani, L. Simulation of Grain Boundary Plasticity, Crack Initiation, and Crack Propagation in an Al-Mg Alloy with Bimodal Grain Size. *Submitt. to Eur. J. Mech. - A/Solids* (2014).
19. Marin, E. On the formulation of a crystal plasticity model. (2006).
20. Pouillier, E., Gourgues, A.-F., Tanguy, D., and Busso, E. P. A study of intergranular fracture in an aluminium alloy due to hydrogen embrittlement. *Int. J. Plast.* 34, 139–153 (2012).
21. ASM International. *Atlas of stress-strain curves*. (ASM International, 2002).
22. Kaufman, J. G. *Properties of Aluminum Alloys*. (ASM International, 1999).
23. Simmons, G., and Wang, H. *Single crystal elastic constants and calculated aggregate properties*. (MIT Press, 1965).
24. Topping, T. D., Hu, T., Manigandan, K., Srivatsan, T. S., and Lavernia, E. J. Quasi-static deformation and final fracture behaviour of aluminium alloy 5083: influence of cryomilling. *Philos. Mag.* 93, 899–921 (2013).